

Article

Physicochemical Characterization of Europium-Doped Hydroxyapatite Thin Films with Antifungal Activity

Carmen Steluta Ciobanu ¹, Mihai Valentin Predoi ², Nicolas Buton ³, Christelle Megier ³, Simona Liliana Iconaru ^{1,*} and Daniela Predoi ^{1,*}

¹ National Institute of Materials Physics, 405A Atomistilor Street, 077125 Magurele, Romania; ciobanucs@gmail.com

² Department of Mechanics, University Politehnica of Bucharest, BN 002, 313 Splaiul Independentei, Sector 6, 060042 Bucharest, Romania; predoi@gmail.com

³ HORIBA Jobin Yvon S.A.S., 6-18, Rue du Canal, CEDEX, 91165 Longjumeau, France; nicolas.buton@horiba.com (N.B.); christelle.megier@horiba.com (C.M.)

* Correspondence: simonaiconaru@gmail.com (S.L.I.); dpredoi@gmail.com (D.P.)

Abstract: Owing to its unique biological and physicochemical properties, hydroxyapatite (HAp) represents one of the most extensively studied biomaterials for biomedical applications. It is well known that *Candida* is currently one of the fungi frequently involved in the onset and development of post-implant infections and, owing to the appearance of antifungal resistance, it is quite difficult to treat despite all the tremendous efforts made in this regard by the scientific world. Therefore, in this context, we report for the first time in this paper, the development and characterization of europium-doped thin films (5EuHAp, $x_{\text{Eu}} = 0.05$) on a Si substrate by a spin-coating method. The results of ultrasound (US), zeta (ζ) potential, X-ray diffraction (XRD), X-ray photoelectron spectroscopy (XPS), transmission electron microscopy (TEM), scanning electron microscopy (SEM), and Fourier-transform infrared spectroscopy (FTIR) studies are presented. The XRD studies conducted on 5EuHAp suspension revealed the nanometric dimensions of the particles and sample purity. In addition, a moderate stability of the 5EuHAp suspension was observed. XPS measurements revealed the presence of Eu 3d in the 5EuHAp thin films. In the SEM micrographs, the surface uniformity and the absence of the surface defects could be observed. Moreover, the results of the FTIR studies showed the presence of the vibrational bands specific to the HAp structure in the studied sample. The antifungal activity of the HAp and 5EuHAp suspensions and coatings was evaluated using the *Candida albicans* ATCC 10231 (*C. albicans*) fungal strain. The qualitative assays of the antifungal properties of HAp and 5EuHAp coatings were also visualized by SEM and CLSM. The antifungal studies revealed that both 5EuHAp suspensions and coatings exhibited noticeable antifungal activity against *C. albicans* cells.



Citation: Ciobanu, C.S.; Predoi, M.V.; Buton, N.; Megier, C.; Iconaru, S.L.; Predoi, D. Physicochemical Characterization of Europium-Doped Hydroxyapatite Thin Films with Antifungal Activity. *Coatings* **2022**, *12*, 306. <https://doi.org/10.3390/coatings12030306>

Academic Editor: Hideyuki Kanematsu

Received: 24 January 2022

Accepted: 22 February 2022

Published: 24 February 2022

Publisher's Note: MDPI stays neutral with regard to jurisdictional claims in published maps and institutional affiliations.



Copyright: © 2022 by the authors. Licensee MDPI, Basel, Switzerland. This article is an open access article distributed under the terms and conditions of the Creative Commons Attribution (CC BY) license (<https://creativecommons.org/licenses/by/4.0/>).

1. Introduction

At present, one of the most studied biomaterials from the calcium phosphate family is hydroxyapatite (HAp), which has special biological activities (such as biocompatibility, bioactivity, nontoxicity, etc.) and physicochemical characteristics (such as structural affinity to accept various ions as dopants, etc.) [1–5]. In addition, HAp has recently been involved in the development of new drug delivery systems due to its unique properties that can improve the therapeutic effect of drugs [5–7]. In the past few years, researchers' attention was captured by the potential luminescent properties gained by HAp after doping with rare earths (RE) ions. The use of RE ions for doping provides important advantages to the host matrix, including the ability to penetrate deep tissue while preserving the luminescence stability and reduced light scattering and photobleaching [5,6,8].

These new characteristics allow the utilization of HAp in many biomedical fields, such as cell labeling, fluorescent probes, etc. It is well known that the excitation of europium with visible light obtains narrow emission bands. In addition, previous studies have shown that RE ions alone (without being hosted in a matrix) could have significant side effects on the environment (for example, on cells/surrounding tissue) when used for in vivo imaging applications [6,9–11]. Therefore, the utilization of a bioceramic matrix, such as hydroxyapatite, may achieve new biomaterials with superior properties [12]. In the study conducted by I. Ortiz-Gomez and collaborators, it was reported that europium-doped amorphous calcium phosphate nanoparticles with luminescent properties were a promising candidate for the development of new sensors for creatinine quantification in urine [13]. Moreover, the luminescent properties of drug-loaded europium-doped hydroxyapatite (EuHAp), which allow the real-time monitoring of drug release efficiency, make this type of biomaterial suitable for use in bioapplications, such as the treatment of diseases of the skeletal system [14–17].

Although it is well known that *Candida* is currently one of the fungi frequently involved in the onset and development of post implant infections due to the appearance of antifungal resistance. It is quite difficult to treat despite the tremendous efforts made in by the scientific world [18–20]. Consequently, the development of new materials with antifungal properties could represent an alternative route for preventing the occurrence of post-implant fungal infection over the long term [19,21,22].

Our previous studies showed that the antimicrobial activity of europium-doped hydroxyapatite (EuHAp) nanoparticles against various microbial strains (e.g., *Escherichia coli* ATCC 25922, *Pseudomonas aeruginosa* 1397, *Staphylococcus aureus* 0364, *Enterococcus faecalis* ATCC 29212, and *Candida albicans* ATCC 10231) depends on the concentration of europium in the powders [23]. In addition, a study conducted by C.L. Popa et al. [24] reported encouraging results regarding the in vitro biocompatibility of EuHAp nanoparticles with the HEK293 human kidney cell line. Moreover, the literature contains various studies that have highlighted the good cytocompatibility of EuHAp powders with MG-63 cells, HeLa cells, and human gingival fibroblasts, etc. [25]. These unique properties reported for europium-doped hydroxyapatite powders make them the correct candidate for producing implant coatings that minimize the risk of post-operative fungal infections and with enhanced biocompatibility. Thus far, as we have shown, studies have obtained and characterized powders based on hydroxyapatite doped with various concentrations of europium. To the best of our knowledge, no studies have been reported to date on the synthesis and characterization of europium-doped hydroxyapatite thin films. In this context, the aim of this study was to develop the first europium-doped hydroxyapatite (EuHAp) thin films deposited on an Si substrate by a spin-coating technique. Moreover, the results of the complex characterization of the obtained thin films are presented in the paper.

2. Materials and Methods

2.1. Materials

The hydroxyapatite thin films doped with europium ($\text{Ca}_{10-x}\text{Eu}_x(\text{PO}_4)_6(\text{OH})_2$, $x_{\text{Eu}} = 0.05$, 5EuHAp) were obtained from 5EuHAp suspension that was synthesized using calcium nitrate tetrahydrate, $\text{Ca}(\text{NO}_3)_2 \cdot 4\text{H}_2\text{O}$ (Sigma Aldrich, St. Louis, MO, USA, $\geq 99.0\%$), ammonium hydrogen phosphate, $(\text{NH}_4)_2\text{HPO}_4$ (Sigma Aldrich, St. Louis, MO, USA, $\geq 99.0\%$), europium nitrate hexahydrate, $\text{Eu}(\text{NO}_3)_3 \cdot 6\text{H}_2\text{O}$ (Alfa Aesar, Landau, Germany, 99.97% purity), ammonium hydroxide, NH_4OH [Sigma Aldrich, St. Louis, MO, USA, 25% NH_3 in H_2O (T)], ethanol absolute, and double-distilled water.

2.2. Europium-Doped Hydroxyapatite Thin Films Using Spin-Coating Technique

The 5EuHAp suspensions were synthesized as described in previous studies [26–28]. In order to obtain a compound that retains the structure of pure hydroxyapatite the $(\text{Ca} + \text{Eu})/\text{P}$ molar ratio was 1.67. Before obtaining the thin films by spin-coating, the 5EuHAp suspension was aged at 40 °C for 72 h. The stability of the final 5EuHAp sus-

suspension was assessed by ultrasound measurements and zeta potential analysis. The Si wafer (Ted Pella, Inc., Redding, CA, USA) used as substrate ($5\text{ mm} \times 5\text{ mm}$) was degreased with acetone for 15 min in an ultrasonic bath. Then, the Si substrate was washed with deionized water and heat treated at $400\text{ }^{\circ}\text{C}$ for 1 h to remove any contaminants that may have remained on the surface. The coatings were realized by spin-coating (Spin150i, POLLOS, Putten, The Netherlands) of 0.3 mL of 5EuHAp suspension at 3500 rpm for 10 s. The process of creating the coatings was performed three times to obtain a sufficiently thick 5EuHAp film on the Si substrate. Each layer was heat treated in air at $40\text{ }^{\circ}\text{C}$ for 30 min. After the last coating, the treatment at $40\text{ }^{\circ}\text{C}$ in air was followed by calcination at $500\text{ }^{\circ}\text{C}$ for 2 h (heating rate $2\text{ }^{\circ}\text{C}/\text{min}$) to obtain the final 5EuHAp thin film.

2.3. Characterization Methods

The physicochemical properties of the obtained 5EuHAp thin films were investigated through techniques including ultrasound (US), Zeta (ζ) potential, X-ray diffraction (XRD), X-Ray photoelectron spectroscopy (XPS), transmission electron microscopy (TEM), scanning electron microscopy (SEM), and Fourier-transform infrared spectroscopy (FTIR). Moreover, the antifungal activity of HAp and 5EuHAp suspensions and thin films deposited on the Si substrate was evaluated using *Candida albicans* yeast. The antifungal assays emphasized that both 5EuHAp suspensions and coatings exhibited very good antifungal properties against *C. albicans* fungal cells.

In order to evaluate the stability of the 5EuHAp suspension we used non-destructive ultrasound studies [29–31] and zeta potential analysis [32–34]. For a correct assessment of the stability of the suspension by ultrasound measurements, double-distilled water was used as reference. Spectral amplitude as a function of frequency for the suspension in relation to reference fluid and attenuation as a function of frequency were used to evaluate the stability of the suspension. The ultrasound instrument was previously described in detail [27]. Zeta (ζ) potential measurements were obtained at $25 \pm 1\text{ }^{\circ}\text{C}$ using SZ-100 Nanoparticle Analyzer (Horiba-SAS France, Longjumeau, France). The EuHAp suspension was diluted in water 10 times before ζ -potential measurements. Three determinations were recorded for each sample. The Debye-Scherrer equation [$\Gamma_{\text{hkl}} = (0.94 \cdot \lambda) / (D_{\text{hkl}} \times \cos\theta)$] was used to calculate the average particle size [35,36]. In the Debye-Scherrer formula, Γ_{hkl} is the full-width at half-maximum of the X-ray diffraction peak in radians, λ is the wavelength of the X-rays, D_{hkl} is the crystal size, and θ is the Bragg angle of the reflection (002). In order to study the morphology of europium-doped hydroxyapatite suspension by transmission electron microscopy (TEM), a CM 20 instrument (Philips FEI, Eindhoven, The Netherlands) equipped with a Lab6 instrument (operating at 200 kV) was used. Before TEM studies, serial dilutions in double-distilled water were obtained and a drop from final suspension was placed on a copper grid and dried [30]. The distribution of particle size was achieved by measuring about 800 particles.

Information about the morphology of the EuHAp thin films was also obtained through scanning electron microscopy (SEM) studies. For this purpose, a Hitachi S4500 microscope (Hitachi, Tokyo, Japan) was utilized. Moreover, information about the chemical composition of the EuHAp thin films was obtained by energy-dispersive X-ray (EDS) spectroscopy. The EDS spectra were recorded with the aid of an EDAX device (Ametek EDAX Inc., Mahwah, NJ, USA) with which the microscope is equipped. Furthermore, the thickness of the EuHAp coatings was estimated.

Complementary information about the morphology and roughness of the 5EuHAp thin films was attained using atomic force microscopy (AFM) studies. The topography of the 5EuHAp thin films was studied in non-contact mode with the aid of an NT-MDT NTEGRA Probe Nano Laboratory instrument (NT-MDT, Moscow, Russia) with a silicon NT-MDT NSG01 cantilever (NT-MDT, Moscow, Russia) coated with a 35 nm gold layer. The AFM images were collected from a surface area of $2.5 \times 2.5\text{ }\mu\text{m}^2$ at room temperature. The data obtained by AFM studies were processed using Gwyddion 2.59 software (Department of Nanometrology, Czech Metrology Institute, Brno, Czech Republic) [37]. The roughness

of the surface of the EuHAp thin films was also assessed by determining the root mean square roughness (R_{RMS}) parameter.

The mechanical properties of the 5EuHAp thin films were studied using a Q800 DMA (TA Instruments, New Castle, DE, USA). The thin films were cut into a rectangle (20 mm × 6 mm) and used for the measurement of the elongation at break and tensile strength and the determination of the elastic modulus using TA Universal Analysis software (version 5.5.24) [38].

The Fourier-transform infrared spectroscopy (FTIR) studies of europium-doped hydroxyapatite thin films were performed with the aid of Perkin Elmer SP-100 equipment (Waltham, MS, USA). The spectrometer was operated in ATR mode in order to collect the FTIR spectra in the spectral region 400–4000 cm⁻¹ (scan resolution 4 cm⁻¹ and 256 scans).

SCIENCE SES 2002 system (Scienta Omicron, Taunusstein, Germany) and a monochromatic source of Al K α X-ray radiation ($h\nu = 1486.6$ eV) were used to collect XPS data. All samples were recorded as having the carbon (C 1s) peak for sp² carbon at a binding energy of 284.8 eV. All XPS data were processed using the Casa XPS 2.3.14 software [39].

In order to evaluate the proliferation rate, the osteoblast MG-63 cell line (American Type Culture Collection, VA, USA) was used. The cells were seeded onto HAp and 5EuHAp thin films at a density of 3×10^4 per well in 12 plates. The samples were incubated in Dulbecco's modified Eagle's medium (DMEM, Gibco, Grand Island, NY, USA) supplemented with 100 µg/mL streptomycin, 10% fetal bovine serum (FBS, Gibco), and 100 U/mL of penicillin. The cultured thin films were kept in a humidified atmosphere with 5% CO₂ at 37 °C for 1, 2, and 4 days. The quantitative evaluation of the proliferation rate of MG-63 cells on HAp and 5EuHAp thin films was then realized. Healthy cells were counted in five different fields per specimen under a microscope (Carl Zeiss, GMBH, Wien, Austria). The in vitro experiments were performed in triplicate for each type of material. Here, the data were presented as the mean ± SD (standard deviation).

The in vitro antifungal properties of 5EuHAp suspensions and coatings were evaluated using the reference fungal strain *Candida albicans* ATCC 10231 (ATCC, Manassas, VA, USA). The experiments were performed using fungal suspensions of *C. albicans* with a concentration of $\sim 5 \times 10^6$ colony forming units (CFU)/mL obtained from 24 h microbial cultures, as previously reported in [40]. The qualitative evaluation of the antifungal activity of HAp and 5EuHAp coatings was performed for three different incubation periods (24, 48, and 72 h) by the visualization of *C. albicans* fungal cells on the surface of HAp and 5EuHAp coatings using scanning electron microscopy (SEM) and confocal laser scanning microscopy (CLSM). The sample preparation for the SEM and CLSM visualization was performed as previously described in [41]. The 3D representation of the SEM and CLSM images were obtained using ImageJ software (Image J 1.51j8) [42]. The quantitative assays of the antifungal activity of HAp and 5EuHAp suspensions and coatings were performed using an adapted method (E2149-10; ASTM International) [43]. The positive control (C+) was a well containing only the fungal suspension. The experiments were performed in triplicate and the results were presented as mean ± SD. The statistical analysis of the data was performed using ANOVA single-factor test.

3. Results

The ultrasonic signals have a central frequency of 5 MHz. These signals were recorded in a coaxial face-to-face placement of the ultrasonic transducers, with the suspension between them in a cubic box. Every 5 s, a new signal was recorded, thus providing information about the time evolution of the suspension. The recorded ultrasonic signals were analyzed, to compute their frequency spectrums, which were compared with equivalent spectrums of the reference liquid (double-distilled water).

Relevant information is obtained as the difference between each spectral amplitude A of a signal through the suspension and A_{ref} of the reference fluid, and this difference is then plotted relative to A_{ref}. Plots below zero mean the suspension is attenuating the signal more than in the reference liquid, which is to be expected (Figure 1a). More important is

the spreading of the curves, which are very narrow, indicating a stable suspension. For such a stable suspension, the spectra of the recorded signals can be averaged. When the attenuation in the reference liquid is known, the relative amplitudes determined before can be used to compute the ultrasonic signal attenuation in the test suspension, measured in nepper/m. The resulting attenuations are depicted in Figure 1b and are compared to those of the reference liquid. Increasing attenuation with increasing frequency is the normal behavior. However, there is a lower than expected attenuation for low frequencies (2 to 3 MHz), which provides information about the small size of the particles which have less influence on ultrasounds at lower frequencies.

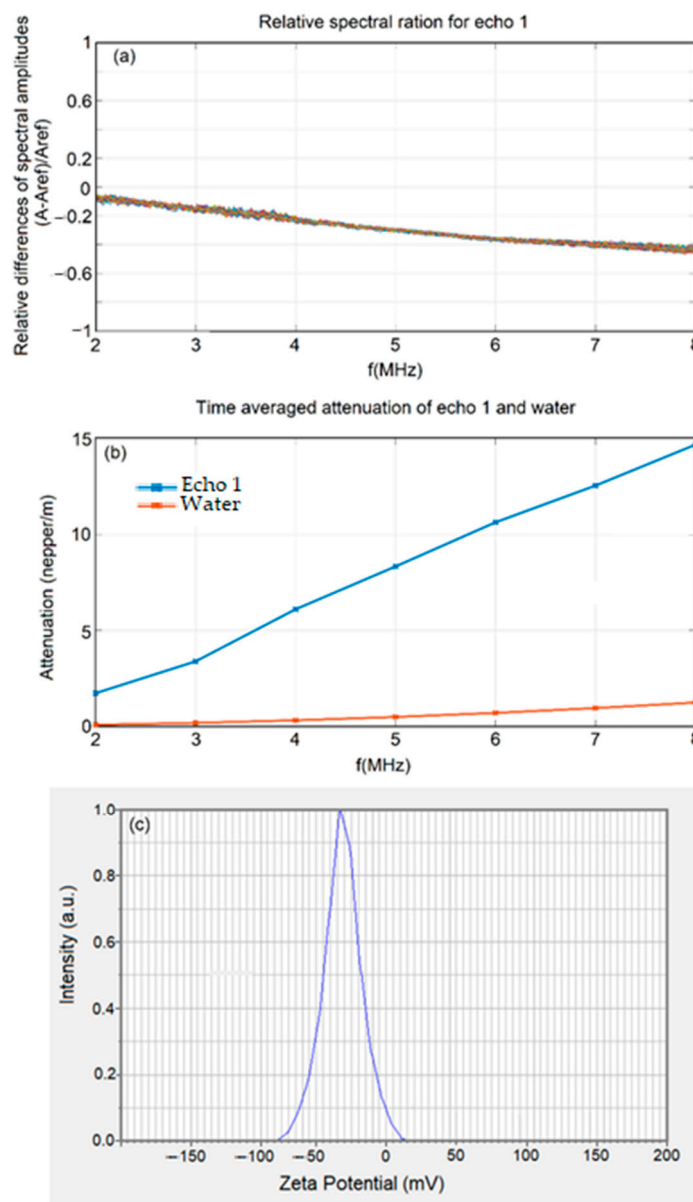


Figure 1. Relative spectral amplitude as a function of frequency (a), attenuation as a function of frequency (b), and zeta potential (ξ) of 5EuHAp suspension (c).

The evaluation of the stability of the 5EuHAp suspension was also achieved by measurement of the zeta potential, a classical method of analysis (Figure 1c). It is known that zeta potential plays an important role in determining the stability of suspensions. The disadvantage of this method is that the analysis is performed on dilute suspensions (in this

case, the 5EuHAp suspension was diluted 10 times). The zeta potential of the 5EuHAp suspension was 35.6 mV, indicating the moderate stability of the 5EuHAp suspension.

The morphology of europium-doped hydroxyapatite suspension was evaluated by transmission electron microscopy (TEM). In Figure 2, the micrographs and the particle size distribution obtained by TEM are obtained. In the TEM micrographs specific to the europium-doped hydroxyapatite nanoparticles (Figure 2a) the nanometric dimension along with their elongated morphology are highlighted. In addition, it could be seen that the nanoparticles have a pronounced tendency to form agglomerates, this behavior being most likely due to the small size of the nanoparticles. The estimation of mean particle size determined by TEM measurements is presented in Figure 2b. The mean particle size obtained for europium-doped hydroxyapatite nanoparticles was 22 ± 1 nm.

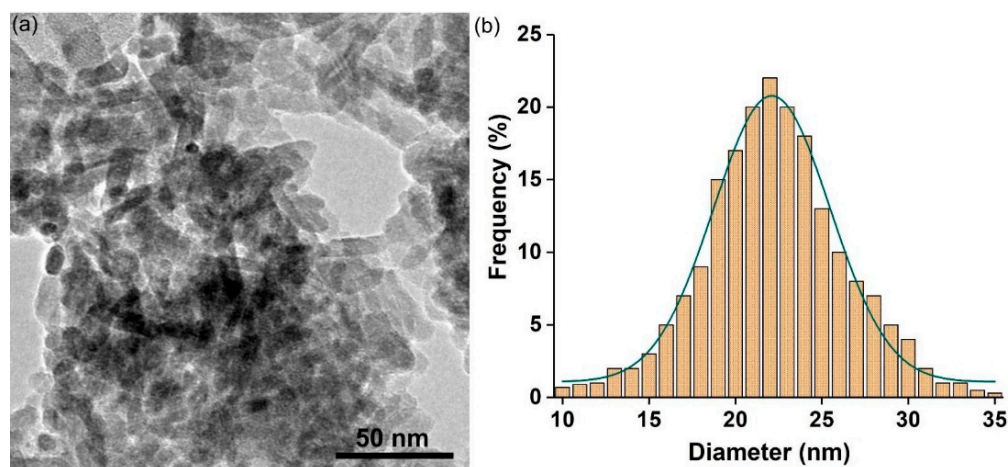


Figure 2. TEM micrographs (a) and particle size distribution (b) specific to 5EuHAp suspensions.

Figure 3 revealed X-ray diffractograms of the 5EuHAp powder (a) and 5EuHAp thin film (b). The crystallite sizes and lattice parameters of the HAp phase obtained for the 5EuHAp powder are presented in Table 1. The powder resulting from the centrifugation of the 5EuHAp suspension was dried at 700 °C and analyzed by X-ray diffraction. The diffraction peaks associated with planes (300) and (002) of 5EuHAp (Table 1) were used to calculate the particle size and lattice constants [44,45]. The results obtained from XRD analysis showed that the nanoparticles of 5EuHAp increased preferentially along with the a-axis of its crystal plane, resulting in ellipsoidal nanoparticles. The slight variation in the parameters of the unit cell could be due to both the deformation that occurs during the process of obtaining the 5EuHAp suspensions and the substitution of calcium ions with those of europium in the structure of hydroxyapatite. The results show that the XRD data for the 5EuHAp powder confirm the data obtained from the TEM analysis of the 5EuHAp suspension.

Table 1. Lattice constant and crystalline sizes calculated from the XRD patterns of the synthesized 5EuHAp suspension and thin film.

| Sample | Lattice Constant | | Crystalline Size | |
|----------------------|------------------|-------|----------------------|----------------------|
| | a (Å) | c (Å) | d ₃₀₀ (Å) | d ₀₀₂ (Å) |
| HAp (JCPDS No.9-432) | 9.416 | 6.874 | | |
| 5EuHAp powder | 9.452 | 6.873 | 7.65 | 21.13 |
| 5EuHAp thin film | 9.450 | 6.870 | 7.60 | 20.98 |

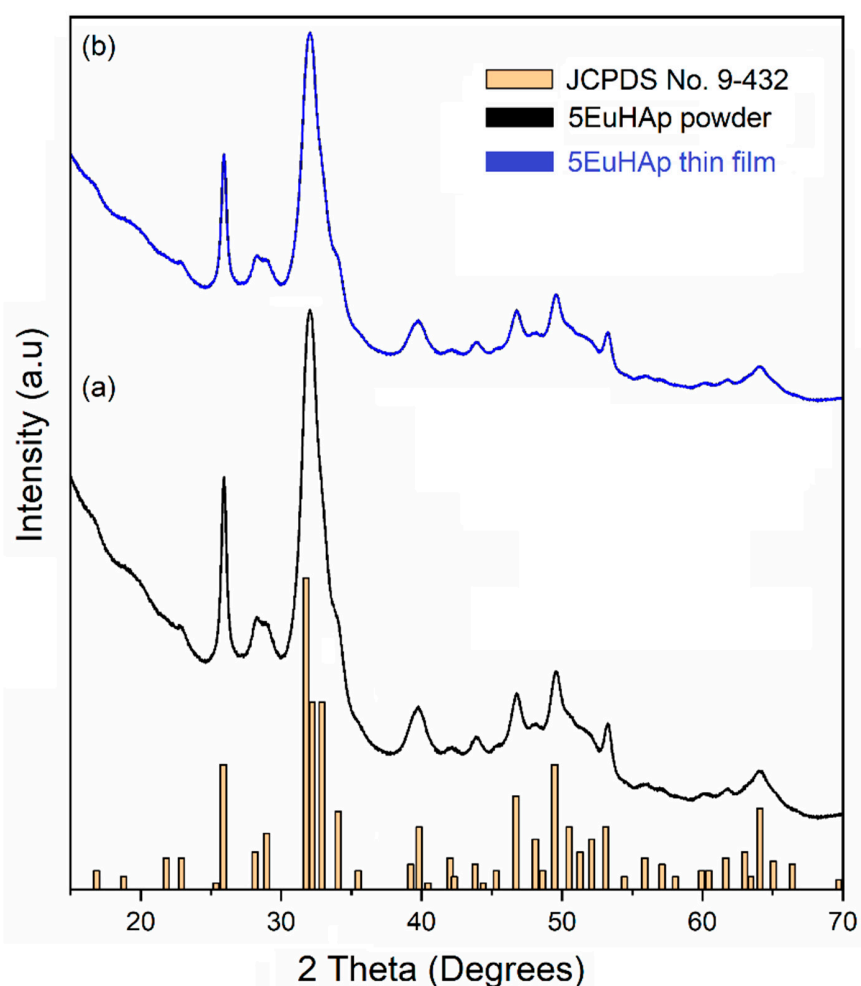


Figure 3. XRD patterns of the 5EuHAp powder (a) and 5EuHAp thin film (b).

Complementary studies of the surface morphology of the 5EuHAp thin films were performed using AFM. The AFM topographies of the 5EuHAp thin films recorded in non-contact mode at room temperature on a surface of $2.5 \times 2.5 \mu\text{m}^2$ are depicted in Figure 4b. The AFM surface topography of the 5EuHAp thin films showed that their surface is typically a homogenous and uniform layer. Moreover, the AFM image also suggested that the 5EuHAp thin films do not present any unevenness, or other visible fissures or cracks on their surface. In addition, the roughness of the 5EuHAp surface was determined from the AFM topography. The value of the R_{RMS} roughness parameter for the entire measured surface was $21.23 \pm 2.6 \text{ nm}$. The results of the AFM studies also emphasized that the 5EuHAp thin film surface is continuous and composed of agglomerations of nanoparticles.

The thickness of the 5EuHAp thin films (Figure 4a) was evaluated from the cross-section image obtained by SEM. Our studies revealed that the coatings thickness is about $141 \pm 10 \text{ nm}$. Figure 4c shows a typical stress-strain curve of the 5EuHAp thin film. The Young's modulus (MPa), tensile strength (MPa), and elongation at break (%) of the 0.05EuHAp thin film were 43.3 ± 6.72 , 1.02 ± 0.18 , and 3.98 ± 0.58 , respectively.

In order to determine the surface components of the 5EuHAp thin film, the XPS technique was used. Figure 5 shows the XPS general spectrum of the 5EuHAp thin film (Figure 5a) and high-resolution XPS spectrum of Eu 3d (Figure 5b). In the XPS general spectrum of the 5EuHAp thin film, the spectral lines of Ca 2p, P 2p, O 1s, Eu 3d, and C 1s were revealed. The binding energy (BE) of Ca 2p, P 2p, and O 1s were 347.3, 133.09, and 532.1 eV, respectively. The spectral line at 284.8 eV was associated with C 1s. The spectral

line observed at 1132.8 eV associated with Eu 3d was in good agreement with previous studies [46] and confirmed the presence of Eu^{3+} in the sample.

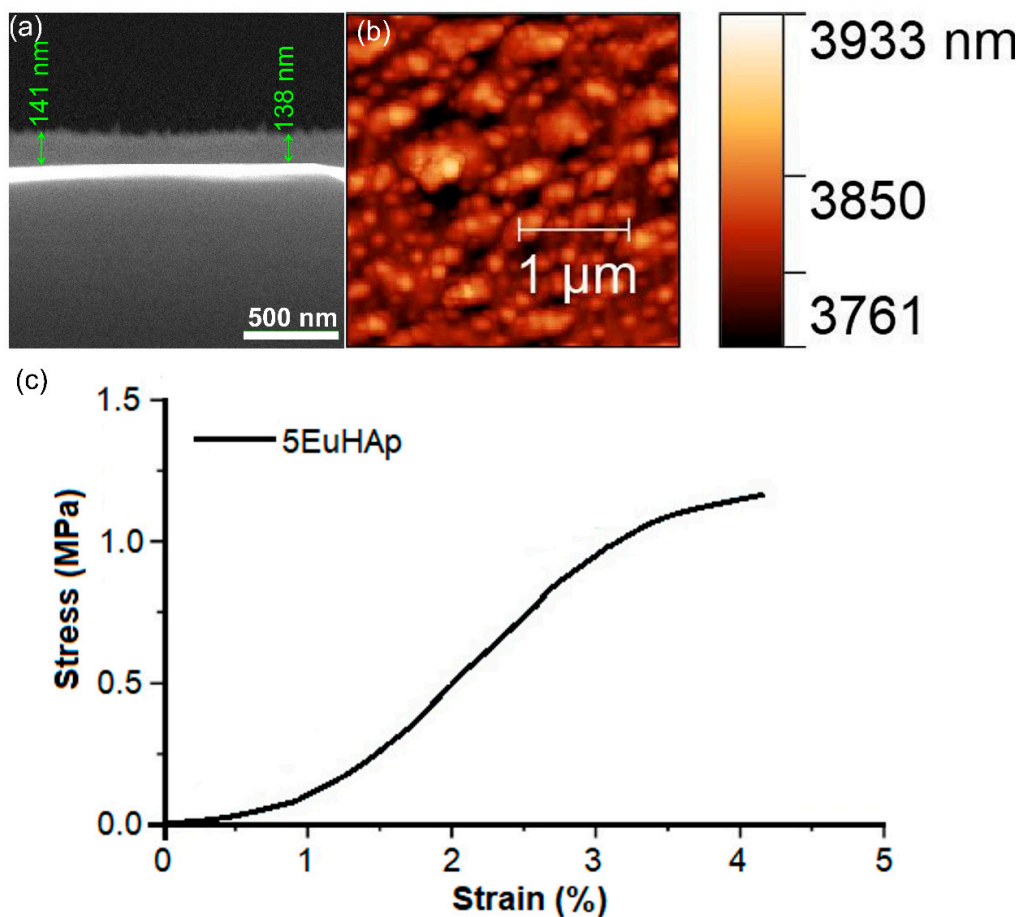


Figure 4. 5EuHAp thin film thickness (a), typical 2D AFM images (b), and stress–strain curves (c).

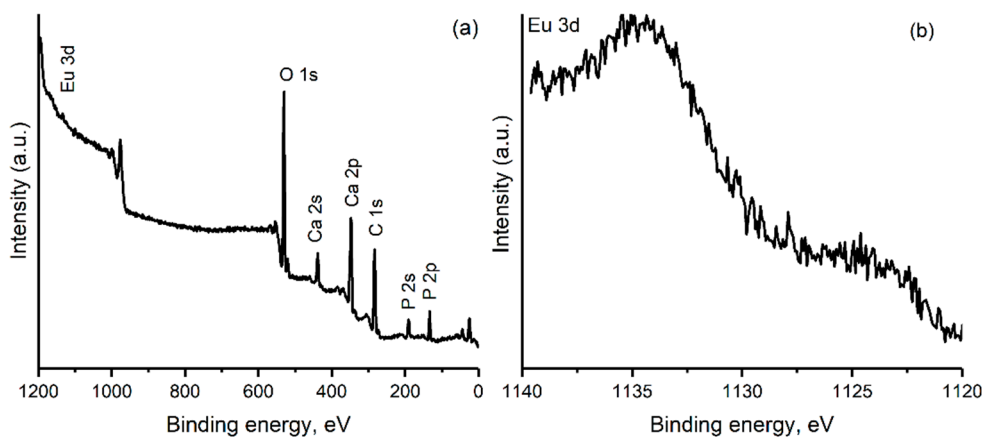


Figure 5. XPS general spectrum of 5EuHAp thin film (a) and high-resolution XPS spectrum of Eu 3d (b).

The surface morphology of the synthesized EuHAp thin films on the Si substrate, together with the EDS spectra are presented in Figure 6a,b. Figure 4a shows that the surface of the studied thin film was continuous and homogenous. The presence of cracks or other surface defects was not observed. Therefore, the spin-coating technique used could obtain thin films with a flawless surface.

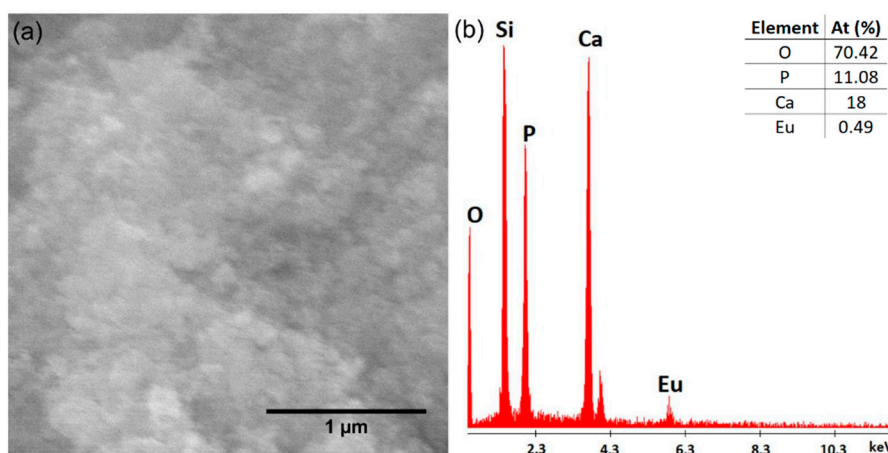


Figure 6. SEM micrographs (a) and EDS spectra (b) of europium doped hydroxyapatite thin films.

EDS spectroscopy obtains information regarding the chemical composition of the samples. The characteristic EDS spectrum of the europium-doped hydroxyapatite thin films is presented in Figure 6b. Our results indicate the presence of calcium (Ca), phosphorus (P), europium (Eu), and oxygen (O) in the studied sample. All these chemical elements are the main components of the EuHAp structure. The presence of the Si line is due to the substrate on which the deposition was made. Moreover, the lack of impurities in the sample is highlighted by the absence of additional lines in the EDS spectrum.

In Figure 7, the results of the FTIR studies conducted on hydroxyapatite (HAp) and europium-doped hydroxyapatite thin films ($x_{\text{Eu}} = 0.05$) are shown as a 3D representation. The following data present only the maxima that have been identified in the FTIR spectrum of HAp. All the main maxima that are observed in the spectra were assigned to the vibrational modes of (PO_4^{3-}) and (OH^-) groups from the HAp structure. Therefore, the weak band at 473 cm^{-1} is characteristic to the doubly degenerate (ν_2) bending mode of (PO_4^{3-}) groups. Moreover, the bands that could be found at 564 and 602 cm^{-1} were due to the ν_4 (triply degenerate) molecular vibration of the O–P–O bond and their presence in the FTIR spectra indicate that the hydroxyapatite is well structured [23,24,26,47]. The peaks from 632 and 3568 cm^{-1} are attributed to the vibrational (ν_L) and stretching (ν_s) vibrational modes of the (OH^-) group. The maxima that could be noticed at around 874 cm^{-1} is due to the presence of (HPO_4^{2-}) groups in the analyzed sample [23,24,26,47].

The presence of the vibrational band at 961 cm^{-1} is specific to the ν_1 molecular vibration of the phosphate group. In the spectral domain that is usually specific to the triply degenerate asymmetric stretching mode vibration (ν_3) of the (PO_4^{3-}) grit is observed the presence of two important maxima is observed at around 1031 and 1091 cm^{-1} , respectively. Furthermore, the presence of broad vibrational bands at 1637 and 3428 cm^{-1} indicate the presence of lattice water molecules in the samples [23,24,26,47]. Therefore, our results revealed that the synthesized samples are pure, without indicating the presence of additional vibrational bands that could be attributed to the impurities. Furthermore, the FTIR results highlighted that the presence of europium in the samples induced a slight displacement of the vibration bands position, together with their broadening.

The results presented in Figure 8 highlight that the proliferation of osteoblasts (MG-63 cells) is highly promoted in both the cases of HAp and 5EuHAp thin films. In addition, it was noticed that the best proliferation rate is obtained after an incubation period of 4 days.

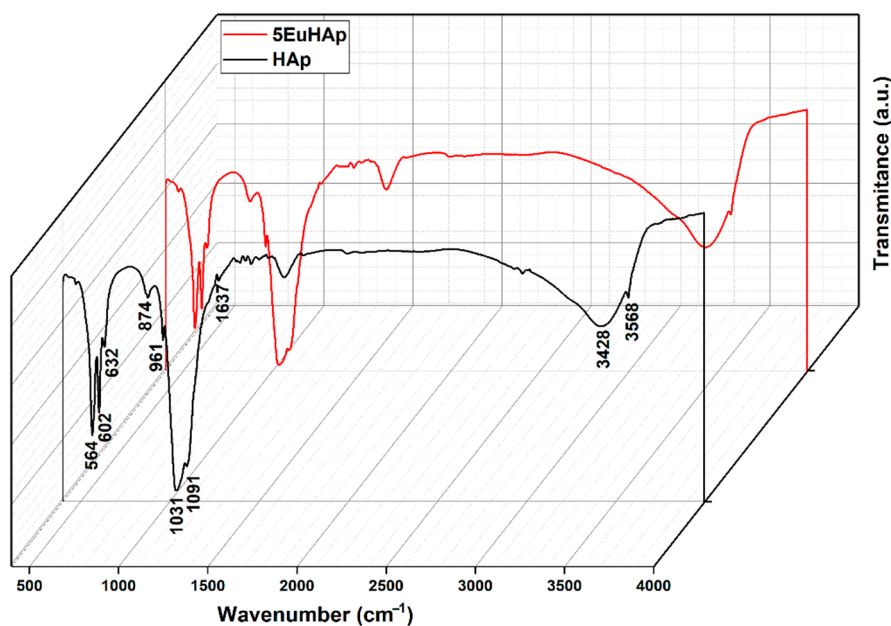


Figure 7. 3D representation of FTIR spectra obtained on hydroxyapatite and europium-doped hydroxyapatite thin films ($x_{\text{Eu}} = 0.05$) deposited on Si substrate.

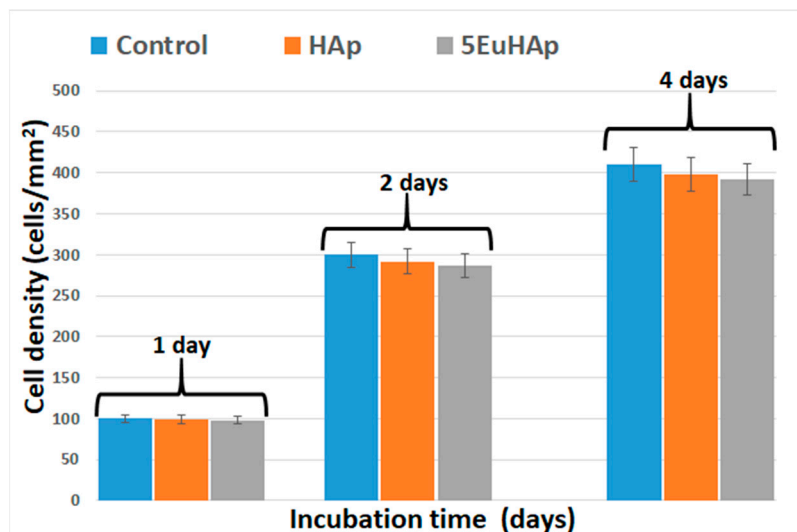


Figure 8. Cell density of osteoblasts (MG-63 cells) on HAp and 5EuHAp thin films for different incubation times.

As can be seen in Figure 8, the maximum cell number is achieved after 4 days of incubation (409 ± 24 for control, 397 ± 19 for the HAp, and 391 ± 20 for the 5EuHAp thin films). Moreover, there is no significant difference between the cell density value obtained for the HAp thin films and the cell density value obtained in the case of the 5EuHAp samples, which suggests that the presence of europium in samples does not alter the proliferation of MG-63 cells. Therefore, it can be seen that the results obtained in the case of europium-doped hydroxyapatite thin layers are similar to those obtained in the case of EuHAp powders [48]. Therefore, we can say that the good biocompatibility of EuHAp powders is preserved even in the case of 5EuHAp thin films.

The antifungal activity of the HAp and 5EuHAp coatings was evaluated with the aid of SEM and CLSM techniques. These techniques allowed the gathering of information regarding the adhesion and proliferation of *C. albicans* cells on the surface of HAp and

5EuHAp coatings. The development and adhesion of the *C. albicans* fungal cells on the surface of HAp and 5EuHAp coatings were evaluated over three incubation periods (24, 48, and 72 h). The data acquired by SEM visualization of the fungal cells adhered on the surface of HAp and 5EuHAp coatings after incubation for 24, 48, and 72 h are presented in Figure 9a–l. The 2D SEM images highlighted that the fungal cells adhered on the surface of the tested coatings present a morphology characteristic to *C. albicans* fungal strain, having round-to-oval shapes and sizes in the range 2.25 to 4.69 μm . The SEM observations have revealed that the HAp coatings did not inhibit the attachment, development, and proliferation of fungal cells on their surface. Moreover, the data suggested that HAp coatings favored the development and proliferation of *C. albicans* cells over all the tested time intervals. In addition, the 3D representation of the SEM data emphasized that the HAp also supported the organization of fungal cells into a fungal biofilm. On the other hand, the SEM visualization showed that the 5EuHAp coatings inhibited the adherence and fungal cell development after incubation for 24 h. In addition, the SEM images also depicted that the 5EuHAp coatings did not allow the fungal cells to develop a fungal biofilm, even after incubation for 24 h. Furthermore, the SEM visualization suggested that the antifungal activity of the 5EuHAp coatings is correlated with the incubation time by clearly presenting that the number of fungal cells adhered on the surface of 5EuHAp coatings significantly decreased with an increase in the incubation time. The SEM visualization evidenced that the number of *C. albicans* fungal cells adhered to the surface of 5EuHAp coatings was considerably reduced after incubation for 48 and 72 h. In addition, the SEM analysis revealed that the 5EuHAp coatings prevented the formation of fungal biofilms on their surfaces. Moreover, after incubation for 72 h, the number of adhered fungal cells was barely noticeable. Moreover, the 3D representations of the SEM images obtained using ImageJ software (Image J 1.51j8) [42] are also depicted in Figure 9d–f,j–l, and emphasized that 5EuHAp inhibited the biofilm formation and that the number of adhered cells decreased significantly with the increase in incubation time.

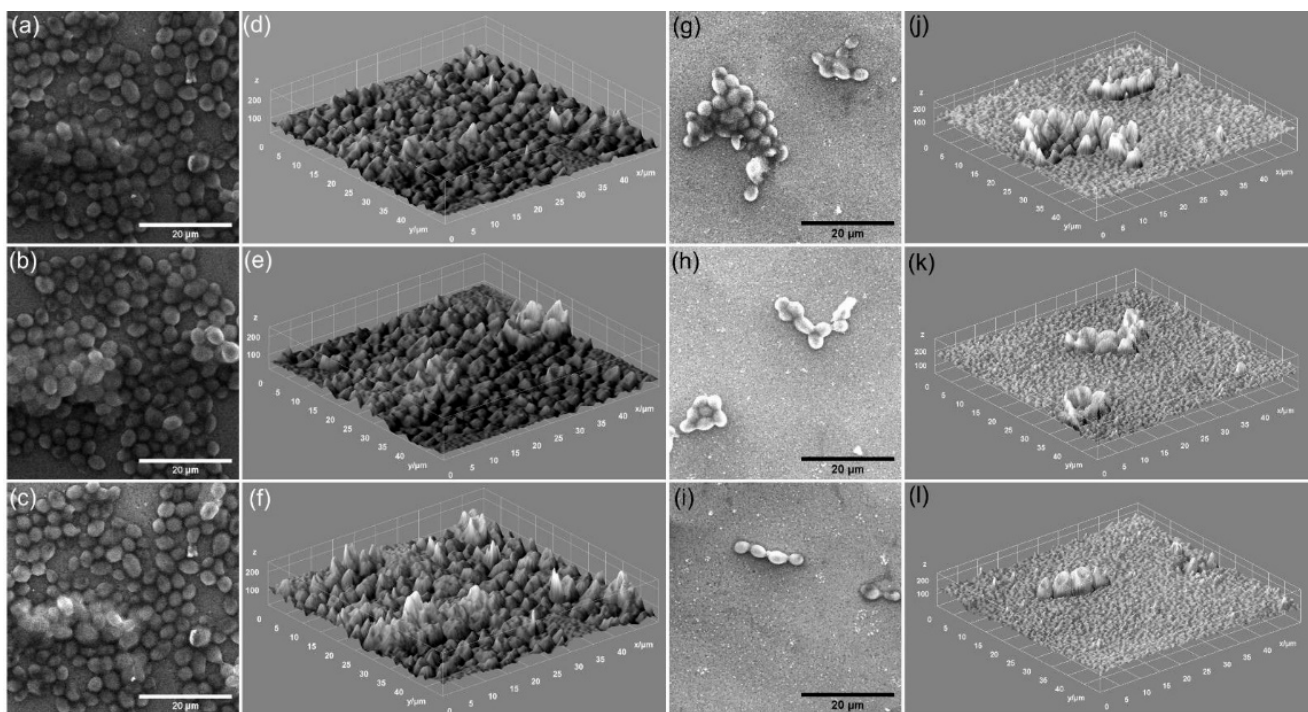


Figure 9. 2D SEM images and 3D representation of *Candida albicans* ATCC 10231 cell development on HAp (a–f) and 5EuHAp (g–l) coatings deposited on Si after 24 h (a,d,g,j) 48 h (b,e,h,k), and 72 h (c,f,i,l) of incubation.

Complementary information regarding the adherence of the *C. albicans* fungal cells on the surface of HAp and 5EuHAp coatings was also obtained by CLSM studies. The CLSM visualization evidenced that the 5EuHAp coatings were effective in preventing fungal biofilm formation for all the three tested time intervals. The CLSM 2D composite images and their 3D representation are depicted in Figure 10a–l. The CLSM observation depicted that HAp coatings promoted the adherence and development of the fungal cells on their surface. In addition, the data also highlighted that the HAp helped the proliferation of fungal cells and positively influenced biofilm formation. These results are in good agreement with the SEM observations. Furthermore, the CLSM results highlighted that the 5EuHAp coatings were effective in inhibiting the fungal cell adherence and proliferation of their surface after incubation for 24 h. Moreover, the CLSM visualization also emphasized that cells attached on the 5EuHAp surfaces were unevenly distributed and did not present any major conglomerates. In addition, the CLSM visualization showed that the cells adhered to the coating's surface have the morphological characteristics of *C. albicans* fungal cells, with an ovaloid shape and sizes from 2.24–4.38 μm . Moreover, the CLSM studies confirmed the SEM results and exhibited that 5EuHAp coatings successfully inhibited the development of *C. albicans* fungal cells on their surface and also that they succeeded in preventing biofilm formation. In addition, the CLSM visualization depicted that after 72 h of incubation, the number of fungal cells adhered to the coating's surface is scarce. Furthermore, the 3D representation of the CLSM images presented in Figure 10d–f, j–l show the structure and spatial distribution of the fungal cells on the surface of 5EuHAp coatings after three different incubation periods. The images depict the spatial distribution of the ovaloid fungal cells (red color) adhered on the surface of 5EuHAp coatings. The 3D representation of the CLSM images also presented in Figure 10 suggests that the development of the fungal cells has been considerably decreased and that their inhibition was affected by the incubation time period. The results obtained of the qualitative antifungal assays performed by visualization using SEM and CLSM techniques concluded that these 5EuHAp coatings have the potential to be of great interest for the future development of antifungal medical devices.

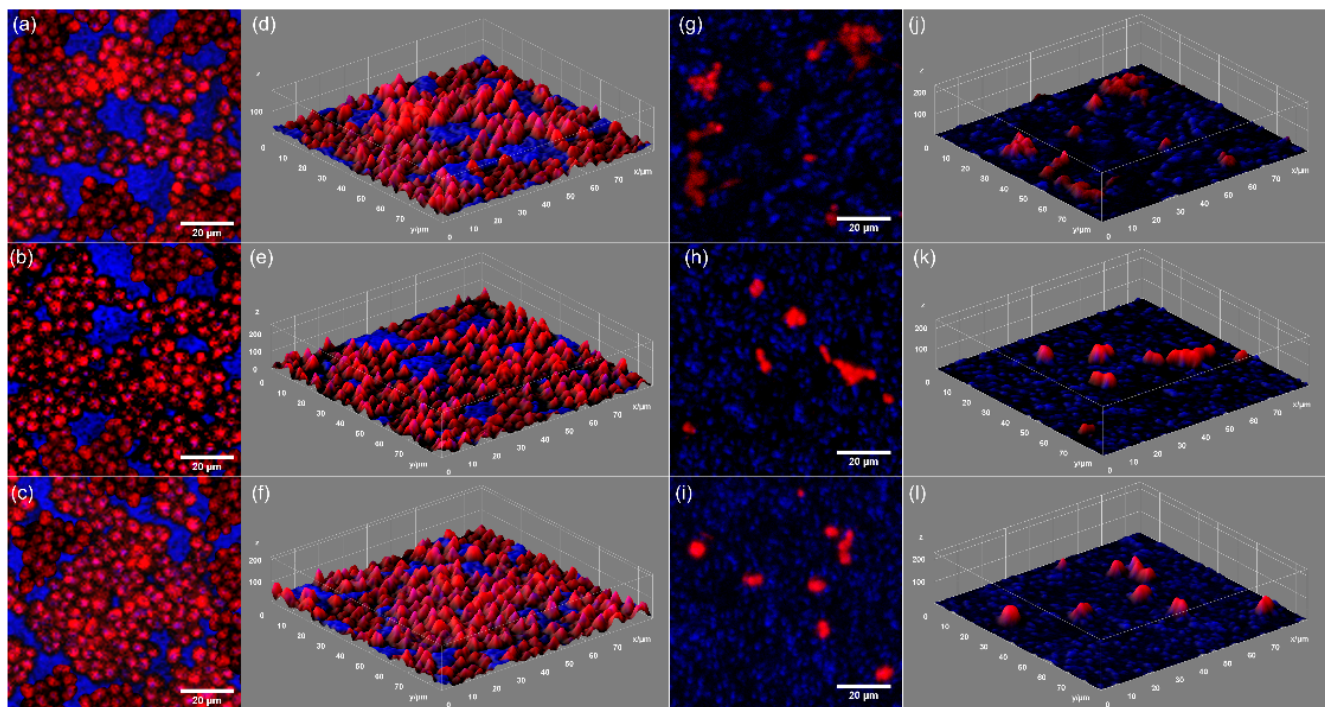


Figure 10. 2D images and 3D representations of the CLSM images of *Candida albicans* ATCC 10231 adhesion on HAp (a–f) and 5EuHAp (g–l) coatings deposited on Si after incubation for 24 h (a,d,g,j), 48 h (b,e,h,k), and 72 h (c,f,i,l).

To obtain additional information about the antifungal activity of 5EuHAp coatings and suspension, quantitative antifungal assays of the suspensions and coatings were also performed using the *C. albicans* ATCC 10231 fungal strain. The results of the quantitative assays are depicted as the graphical representation of the effects of 5EuHAp suspensions and coatings on the development of *C. albicans* ATCC 10231 colony-forming units (CFU) for 24, 48, and 72 h and are presented in Figure 11.

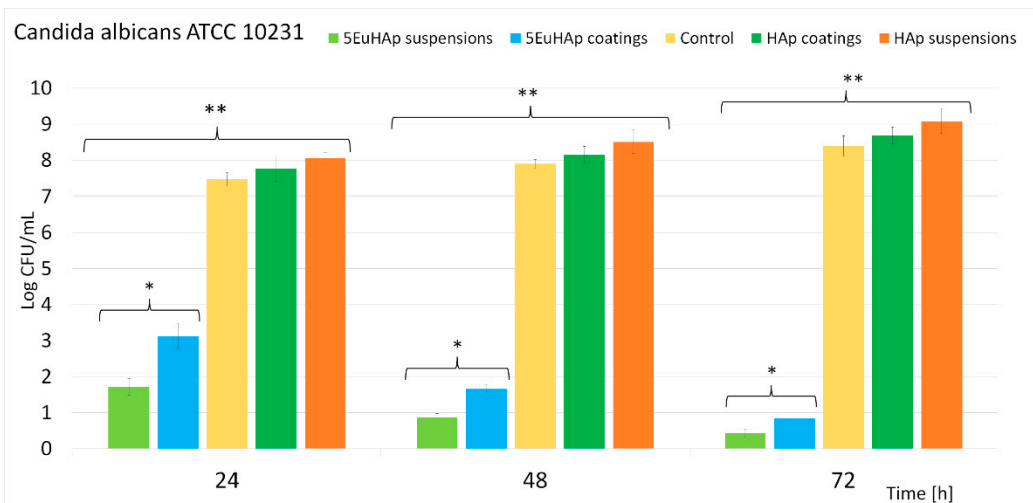


Figure 11. Antifungal activity of HAp and 5EuHAp suspensions and coatings on the development *Candida albicans* ATCC 10231 fungal cells over different incubation periods. The results are presented as mean \pm SD. Statistical analysis was performed by one-way ANOVA. The determined *p*-values: * *p* \leq 0.002, ** *p* \leq 0.0001.

The results of the quantitative assays highlighted that the inhibition of the fungal cells was achieved from the first phase of adherence in both the suspension and coatings. The colony forming unit count (CFUc) assay showed that there was a noticeable decrease in the number of colonies after 24 h for both 5EuHAp suspensions and coatings compared to the number of colonies formed in the case of the positive control culture (C+). Furthermore, in good agreement with the qualitative assays, the quantitative studies suggested that the antifungal activity of both suspensions and coatings was influenced by the incubation period. Moreover, the results showed that after 72 h, both the suspensions and the coatings exhibited good antifungal activity and caused a significant reduction of the number of CFUs. These results are in good agreement with previously reported data on europium-doped hydroxyapatite powders with antimicrobial properties [23]. The antifungal assays also suggested that the 5EuHAp suspensions exhibited better antifungal activity compared to 5EuHAp coatings. These results are also in good agreement with previously reported studies regarding coatings that almost completely retain the antifungal effects of the suspensions used for their depositions [40,49]. The preliminary results obtained from the in vitro antifungal assays highlighted that both 5EuHAp suspensions and coatings present strong antifungal properties that are correlated with the incubation time. In addition, the results of the qualitative assays performed by SEM and CLSM visualizations showed that the adhesion and development of *C. albicans* fungal cells was effectively inhibited by 5EuHAp coatings. Moreover, the SEM and CLSM visualizations also highlighted that the 5EuHAp coatings were effective in preventing fungal biofilm formation. The antifungal studies performed on HAp suspensions and coatings demonstrated that HAp suspensions and coatings did not have the ability to inhibit the development and proliferation of the *C. albicans* fungal cells. In addition, the results also suggested that the both HAp suspensions and coatings had a positive influence on the development of the fungal cells and that favored their proliferation for all the tested time intervals. These results are also supported by the qualitative studies performed by SEM and CLSM visualization

and also by previous reported studies on the antimicrobial properties of hydroxyapatite suspensions and hydroxyapatite coatings [27,33,50]. In addition, the data also suggested that the antifungal properties of the 5EuHAp suspensions and coatings could be attributed to the presence of europium ions from the hydroxyapatite lattice. Therefore, the results showed that the development of novel 5EuHAp suspensions and coatings could lead to the development of promising novel antifungal medical devices.

4. Conclusions

In this paper, we report for the first time the synthesis of europium-doped thin films by a spin-coating method. In addition, the physicochemical and antifungal properties of the obtained sample were reported. Our results highlighted the moderate stability of the 5EuHAp suspension. The results of the complex studies conducted on the obtained samples indicate their purity. The presence of Eu³⁺ in the samples was also highlighted. The main vibrational bands can be assigned to the molecular vibration of phosphate and hydroxyl groups from the HAp structure. The qualitative in vitro antifungal studies emphasized that 5EuHAp coatings inhibited the adhesion and development of *C. albicans* fungal cells for all the tested time intervals. Our studies also highlighted that the 5EuHAp coatings were effective in preventing *C. albicans* fungal biofilm formation. In addition, the quantitative assays also demonstrated that the 5EuHAp suspensions used for the coatings exhibited good antifungal activity against *C. albicans*. Furthermore, the in vitro analysis of the HAp suspensions and coatings revealed that the antifungal properties of the 5EuHAp was most likely attributable to the presence of the europium ions in the HAp lattice, as the HAp alone did not inherently exhibit any antifungal properties. Our results suggest that 5EuHAp can represent a promising candidate for covering implants in order to prevent the adhesion and development of *C. albicans* fungal cells.

Author Contributions: Conceptualization, C.S.C., M.V.P., S.L.I. and D.P.; methodology, C.S.C., M.V.P., S.L.I. and D.P.; software, M.V.P.; validation, C.S.C., M.V.P., S.L.I. and D.P.; formal analysis, C.S.C., M.V.P., S.L.I., C.M., N.B. and D.P.; investigation, C.S.C., M.V.P., S.L.I., C.M., N.B. and D.P.; resources, M.V.P., S.L.I., C.M., N.B. and D.P.; data curation, C.S.C., S.L.I. and D.P.; writing—original draft preparation, C.S.C., M.V.P., S.L.I., N.B. and D.P.; writing—review and editing, C.S.C., M.V.P., S.L.I. and D.P.; visualization, C.S.C., M.V.P., S.L.I., C.M., N.B. and D.P.; supervision, S.L.I. and D.P.; project administration, S.L.I., and D.P.; funding acquisition, D.P. All authors have read and agreed to the published version of the manuscript.

Funding: This work was supported by the Romanian Ministry of Research and Innovation through the project PN-III-P2-2.1-PED-2019-0868 contract number 467PED/2020.

Institutional Review Board Statement: Not applicable.

Informed Consent Statement: Not applicable.

Data Availability Statement: Not applicable.

Acknowledgments: We are grateful to Monica Luminita Badea (UASVM Bucharest) for their technical help on evaluation of antifungal activity of europium doped hydroxyapatite against *C. albicans*. We thank to George A. Stanciu and Radu Hristu (Center for Microscopy-Microanalysis and Information Processing, University Politehnica of Bucharest) for their technical support in acquiring the CLSM images.

Conflicts of Interest: The authors declare no conflict of interest.

References

1. Paterlini, V.; Bettinelli, M.; Rizzi, R.; El Khouri, A.; Rossi, M.; Della Ventura, G.; Capitelli, F. Characterization and Luminescence of Eu³⁺- and Gd³⁺-Doped Hydroxyapatite Ca₁₀(PO₄)₆(OH)₂. *Crystals* **2020**, *10*, 806. [[CrossRef](#)]
2. Dorozhkin, S.V. Hydroxyapatite and other calcium orthophosphates: Bioceramics, coatings and dental applications. In *Hydroxyapatite and Other Calcium Orthophosphates: Bioceramics, Coatings and Dental Applications*; Nova Science Publishers: New York, NY, USA, 2017; pp. 1–462.

3. Boanini, E.; Torricelli, P.; Gazzano, M.; Giardinob, R.; Bigi, A. Alendronate hydroxyapatite nanocomposites and their interaction with osteoclasts and osteoblast-like cells. *Biomaterials* **2008**, *29*, 790–796. [[CrossRef](#)] [[PubMed](#)]
4. Sun, Y.; Yang, H.; Tao, D. Microemulsion process synthesis of lanthanide-doped hydroxyapatite nanoparticles under hydrothermal treatment. *Ceram. Int.* **2011**, *37*, 2917–2920. [[CrossRef](#)]
5. Van, H.N.; Tam, P.D.; Kien, N.; Huy, P.T.; Pham, V.H. Enhancing the luminescence of Eu³⁺/Eu²⁺ ion-doped hydroxyapatite by fluoridation and thermal annealing. *Luminescence* **2017**, *32*, 817–823. [[CrossRef](#)] [[PubMed](#)]
6. Mondal, S.; Park, S.; Choi, J.; Vo, T.M.T.; Shin, J.H.; Kang, Y.H.; Oh, J. Rare earth element doped hydroxyapatite luminescent bioceramics contrast agent for enhanced biomedical imaging and therapeutic applications. *Ceram. Int.* **2020**, *46*, 29249–29260. [[CrossRef](#)]
7. Victor, S.P.; Gayathri Devi, M.G.; Paul, W.; Vijayan, V.M.; Muthu, J.; Sharma, C.P. Europium doped calcium deficient hydroxyapatite as theranostic nanoplatforms: Effect of structure and aspect ratio. *ACS Biomater. Sci. Eng.* **2017**, *3*, 3588–3595. [[CrossRef](#)]
8. Doat, A.; Fanjul, M.; Pelle, F.; Hollande, E.; Lebugle, A. Europium-doped bioapatite: A new photostable biological probe, internalizable by human cells. *Biomaterials* **2003**, *24*, 3365–3371. [[CrossRef](#)]
9. Liu, M.; Shu, M.; Yan, J.; Liu, X.; Wang, R.; Hou, Z.; Lin, J. Luminescent net-like inorganic scaffolds with europium-doped hydroxyapatite for enhanced bone reconstruction. *Nanoscale* **2021**, *1*, 1181–1194. [[CrossRef](#)]
10. Zhang, H.; Feng, J.; Zhu, W.; Liu, C.; Xu, S.; Shao, P.; Wu, D.; Yang, W.; Gu, J. Chronic toxicity of rare-earth elements on human beings. *Biol. Trace Elem. Res.* **2000**, *73*, 1–17. [[CrossRef](#)]
11. Hemmer, E.; Venkatachalam, N.; Hyodo, H.; Hattori, A.; Ebina, Y.; Kishimoto, H.; Soga, K. Upconverting and NIR emitting rare earth based nanostructures for NIRbioimaging. *Nanoscale* **2013**, *5*, 11339–11361. [[CrossRef](#)]
12. Kataoka, T.; Shiba, K.; Tagaya, M. Preparation of europium(III)-doped hydroxyapatite nanocrystals in the presence of cationic surfactant. *Colloids Interface Sci. Commun.* **2016**, *13*, 1–5. [[CrossRef](#)]
13. Ortiz-Gómez, I.; Ramírez-Rodríguez, G.B.; Capitán-Vallvey, L.F.; Salinas-Castillo, A.; Delgado-López, J.M. Highly stable luminescent europium-doped calcium phosphate nanoparticles for creatinine quantification. *Colloids Surf. B* **2020**, *196*, 111337. [[CrossRef](#)] [[PubMed](#)]
14. Hou, Z.; Yang, P.; Lian, H.; Wang, L.; Zhang, C.; Li, C.; Chai, R.; Cheng, Z.; Lin, J. Multifunctional hydroxyapatite nanofibers and microbelts as drug carriers. *Chem. Eur. J.* **2009**, *15*, 6973–6982. [[CrossRef](#)] [[PubMed](#)]
15. Shi, D.L.; Lian, J.; Wang, W.; Liu, G.K.; He, P.; Dong, Z.Y.; Wang, L.M.; Ewing, R.C. Luminescent Carbon Nanotubes by Surface Functionalization. *Adv. Mater.* **2006**, *18*, 189–193. [[CrossRef](#)]
16. Lin, Y.S.; Wu, S.H.; Hung, Y.; Chou, Y.H.; Chang, C.; Lin, M.L.; Tsai, C.P.; Mou, C.Y. Multifunctional composite nanoparticles: Magnetic, luminescent, and mesoporous. *Chem. Mater.* **2006**, *18*, 5170–5172. [[CrossRef](#)]
17. Sun, L.N.; Zhang, H.J.; Peng, C.Y.; Yu, J.B.; Meng, Q.G. Covalent Linking of Near-Infrared Luminescent Ternary Lanthanide (Er³⁺, Nd³⁺, Yb³⁺) Complexes on Functionalized Mesoporous MCM-41 and SBA-15. *J. Phys. Chem. B* **2006**, *110*, 7249–7258. [[CrossRef](#)]
18. Lafuente-Ibáñez de Mendoza, I.; Cayero-Garay, A.; Quindós-Andrés, G.; Aguirre-Urizar, J.M. A systematic review on the implication of *Candida* in peri-implantitis. *Int. J. Implant Dent.* **2021**, *7*, 73. [[CrossRef](#)]
19. Gökmənoglu, C.; Kara, N.B.; Beldüz, M.; Kamburoğlu, A.; Tosun, I.; Sadık, E.; Kara, C. Evaluation of *Candida Albicans* biofilm formation on various parts of implant material surfaces. *Niger. J. Clin. Pr.* **2018**, *21*, 33–37. [[CrossRef](#)]
20. Cobo, F.; Rodríguez-Granger, J.; Sampedro, A.; Aliaga-Martínez, L.; Navarro-Marí, J.M. Candida prosthetic joint infection. A review of treatment methods. *J. Bone Jt. Inf.* **2017**, *2*, 114–121. [[CrossRef](#)]
21. Vargas-Blanco, D.A.; Lynn, A.Z.; Rosch, J.; Noreldin, R.; Salerni, A.D.; Lambert, C.; Rao, R.P. A pre-therapeutic coating for medical devices that prevents the attachment of *Candida albicans*. *Ann. Clin. Microbiol. Antimicrob.* **2017**, *16*, 41. [[CrossRef](#)] [[PubMed](#)]
22. Richardson, M.D. Changing patterns and trends in systemic fungal infections. *J. Antimicrob. Chemother.* **2005**, *56*, i5–i11. [[CrossRef](#)] [[PubMed](#)]
23. Iconaru, S.L.; Motelica-Heino, M.; Predoi, D. Study on europium-doped hydroxyapatite nanoparticles by fourier transform infrared spectroscopy and their antimicrobial properties. *J. Spectrosc.* **2013**, *2013*, 284285. [[CrossRef](#)]
24. Popa, C.L.; Ciobanu, C.S.; Iconaru, S.L.; Stan, M.S.; Dinischiotu, A.; Negrila, C.C.; Motelica-Heino, M.; Guégan, R.; Predoi, D. Systematic investigation and in vitro biocompatibility studies on mesoporous europium doped hydroxyapatite. *Cent. Eur. J. Chem.* **2014**, *12*, 1032–1046. [[CrossRef](#)]
25. Tite, T.; Popa, A.C.; Balescu, L.M.; Bogdan, I.M.; Pasuk, I.; Ferreira, J.; Stan, G.E. Cationic Substitutions in Hydroxyapatite: Current Status of the Derived Biofunctional Effects and Their In Vitro Interrogation Methods. *Materials* **2018**, *11*, 2081. [[CrossRef](#)] [[PubMed](#)]
26. Ciobanu, C.S.; Iconaru, S.L.; Massuyeau, F.; Constantin, L.V.; Costescu, A.; Predoi, D. Synthesis, structure, and luminescent properties of europium-doped hydroxyapatite nanocrystalline powders. *J. Nanomater.* **2012**, *2012*, 942801. [[CrossRef](#)]
27. Predoi, D.; Iconaru, S.L.; Predoi, M.V.; Motelica-Heino, M.; Guegan, R.; Buton, N. Evaluation of antibacterial activity of zinc-doped hydroxyapatite colloids and dispersion stability using ultrasounds. *Nanomaterials* **2019**, *9*, 515. [[CrossRef](#)]
28. Ciobanu, C.S.; Iconaru, S.L.; Popa, C.L.; Motelica-Heino, M.; Predoi, D. Evaluation of Samarium Doped Hydroxyapatite, Ceramics for Medical Application: Antimicrobial Activity. *J. Nanomater.* **2015**, *2015*, 849216. [[CrossRef](#)]
29. Predoi, D.; Iconaru, S.L.; Predoi, M.V.; Motelica-Heino, M. Removal and Oxidation of As(III) from Water Using Iron Oxide Coated CTAB as Adsorbent. *Polymers* **2020**, *12*, 1687. [[CrossRef](#)]

30. Predoi, D.; Iconaru, S.L.; Ciobanu, S.C.; Predoi, S.-A.; Buton, N.; Megier, C.; Beuran, M. Development of Iron-Doped Hydroxyapatite Coatings. *Coatings* **2021**, *11*, 186. [CrossRef]
31. Predoi, S.-A.; Ciobanu, C.S.; Motelica-Heino, M.; Chifiriuc, M.C.; Badea, M.L.; Iconaru, S.L. Preparation of Porous Hydroxyapatite Using Cetyl Trimethyl Ammonium Bromide as Surfactant for the Removal of Lead Ions from Aquatic Solutions. *Polymers* **2021**, *13*, 1617. [CrossRef]
32. Iconaru, S.L.; Prodan, A.M.; Buton, N.; Predoi, D. Structural Characterization and Antifungal Studies of Zinc-Doped Hydroxyapatite Coatings. *Molecules* **2017**, *22*, 604. [CrossRef] [PubMed]
33. Predoi, D.; Iconaru, S.L.; Predoi, M.V.; Motelica-Heino, M.; Buton, N.; Megier, C. Obtaining and Characterizing Thin Layers of Magnesium Doped Hydroxyapatite by Dip Coating Procedure. *Coatings* **2020**, *10*, 510. [CrossRef]
34. Prodan, A.M.; Iconaru, S.L.; Predoi, M.V.; Predoi, D.; Motelica-Heino, M.; Turculet, C.S.; Beuran, M. Silver-Doped Hydroxyapatite Thin Layers Obtained by Sol-Gel Spin Coating Procedure. *Coatings* **2020**, *10*, 14. [CrossRef]
35. Debye, P.; Scherrer, P. Interference of irregularly oriented particles in x-rays. *Physik. Z.* **1916**, *17*, 277–283.
36. Debye, P.; Scherrer, P. Interference on inordinate orientated particles in x-ray light. III. *Physik. Z.* **1917**, *18*, 291–301.
37. Gwyddion. Available online: <http://gwyddion.net/> (accessed on 20 January 2022).
38. Deng, L.; Li, Y.; Zhang, A.; Zhang, H. Characterization and physical properties of electrospun gelatin nanofibrous films by incorporation of nano-hydroxyapatite. *Food Hydrocoll.* **2020**, *103*, 105640. [CrossRef]
39. Fairley, N.; Fernandez, V.; Richard-Plouet, M.; Guillot-Deudon, C.; Walton, J.; Smith, E.; Flahaut, D.; Greiner, M.; Biesinger, M.; Tougaard, S.; et al. Systematic and collaborative approach to problem solving using X-ray photoelectron spectroscopy. *Appl. Surf. Sci. Adv.* **2021**, *5*, 100112. [CrossRef]
40. Iconaru, S.L.; Predoi, M.V.; Chapon, P.; Gaiaschi, S.; Rokosz, K.; Raaen, S.; Motelica-Heino, M.; Predoi, D. Investigation of Spin Coating Cerium-Doped Hydroxyapatite Thin Films with Antifungal Properties. *Coatings* **2021**, *11*, 464. [CrossRef]
41. Ciobanu, C.S.; Groza, A.; Iconaru, S.L.; Popa, C.L.; Chapon, P.; Chifiriuc, M.C.; Hristu, R.; Stanciu, G.A.; Negrila, C.C.; Ghita, R.V.; et al. Antimicrobial activity evaluation on silver doped hydroxyapatite/polydimethylsiloxane composite layer. *BioMed Res. Int.* **2015**, *2015*, 926513. [CrossRef]
42. ImageJ. Available online: <http://imagej.nih.gov/ij> (accessed on 10 January 2018).
43. ASTM E2149-13a; Standard Test Method for Determining the Antimicrobial Activity of Antimicrobial Agents under Dynamic Contact Conditions. ASTM International: West Conshohocken, PA, USA, 2013.
44. Danilchenko, S.N.; Kukharenko, O.G.; Moseke, C.; Protsenko, I.Y.; Sukhodub, L.F.; Sulkio-Cleff, B. Determination of the bone mineral crystallite size and lattice strain from diffraction line broadening. *Cryst. Res. Technol.* **2002**, *37*, 1234–1240. [CrossRef]
45. Richardson, J.W.; Faber, J., Jr. *Advances in X-ray Analysis*; Barrett, C.S., Cohen, J.B., Faber, J., Jr., Jenkins, R., Leyden, D.E., Russ, J.C., Predecki, P.K., Eds.; Plenum Publishing: New York, NY, USA, 1986; Volume 29.
46. Predoi, D.; Derible, S.; Duflo, H. Synthesis and ultrasonic characterization of hydroxyapatite ceramic powders. *J. Optoelectron. Adv. Mat.* **2010**, *4*, 110.
47. Markovic, M.; Fowler, B.O.; Tung, M.S. Preparation and Comprehensive Characterization of a Calcium Hydroxyapatite Reference Material. *J. Res. Natl. Inst. Stand. Technol.* **2004**, *109*, 553–568. [CrossRef] [PubMed]
48. Frumosu, F.; Iconaru, S.L.; Predoi, D. Europium concentration effect of europium doped hydroxyapatite on proliferation of osteoblast cells. *Dig. J. Nanomater. Bios.* **2011**, *6*, 1859–1865.
49. Ciobanu, C.S.; Predoi, D.; Chapon, P.; Predoi, M.V.; Iconaru, S.L. Fabrication and Physico-Chemical Properties of Antifungal Samarium Doped Hydroxyapatite Thin Films. *Coatings* **2021**, *11*, 1466. [CrossRef]
50. Predoi, D.; Iconaru, S.L.; Predoi, M.V.; Groza, A.; Gaiaschi, S.; Rokosz, K.; Raaen, S.; Negrila, C.C.; Prodan, A.-M.; Costescu, A.; et al. Development of Cerium-Doped Hydroxyapatite Coatings with Antimicrobial Properties for Biomedical Applications. *Coatings* **2020**, *10*, 516. [CrossRef]